energies

MDPI

Article

Insulation Resistance Degradation Models of Extruded Power Cables under Thermal Ageing

Xufei Ge, Fulin Fan *, Martin J. Given and Brian G. Stewart *

Institute for Energy and Environment, University of Strathclyde, Glasgow G1 1XW, UK; xufei.ge@strath.ac.uk (X.G.); m.given@strath.ac.uk (M.J.G.)

* Correspondence: f.fan@strath.ac.uk (F.F.); brian.stewart.100@strath.ac.uk (B.G.S.)

Abstract: Insulation resistance (IR) is an essential metric indicating insulation conditions of extruded power cables. To deliver reliable IR simulation as a reference for practical cable inspection, in this paper, four IR degradation models for cross-linked polyethylene-insulated cables under thermal ageing are presented. In addition, the influences of methodologies and temperature profiles on IR simulation are evaluated. Cable cylindrical insulation is first divided into sufficiently small segments whose temperatures are simulated by jointly using a finite volume method and an artificial neural network to model the thermal ageing experiment conditions. The thermal degradation of IR is then simulated by dichotomy models that randomly sample fully degraded segments based on an overall insulation (layer) ageing condition estimation and discretization models that estimate the gradual degradation of individual segments, respectively. Furthermore, uniform and non-uniform temperature profiles are incorporated into dichotomy and discretization models, respectively, for a comparison. The IR simulation results are not only compared between different models, but also discussed around the sensitivity of IR simulation to segment sizes and degradation rates. This provides cable assessment engineers with insights into model behaviour as a reference for their selection of appropriate IR degradation models.

Keywords: extruded power cables; insulation resistance; thermal ageing; dichotomy models; discretization models; insulation temperature profiles

Citation: Ge, X.; Fan, F.; Given, M.J.; Stewart, B.G. Insulation Resistance Degradation Models of Extruded Power Cables under Thermal Ageing. *Energies* **2024**, *17*, 1062. https://doi.org/10.3390/en17051062

Academic Editor: Tomasz Norbert Kołtunowicz

Received: 23 December 2023
Revised: 15 February 2024
Accepted: 17 February 2024
Published: 23 February 2024

1. Introduction

The ageing of extruded power cables refers to the gradual deterioration and alteration of their physical, chemical and electrical properties over time subject to environmental, thermal, mechanical and electrical stresses. The ageing process can result in a gradual reduction in the cable performance, including its insulation integrity, mechanical strength and overall reliability. Factors such as temperature variations, exposure to moisture, chemical interactions, mechanical stresses and electrical loading contribute to the cable ageing process, potentially diminishing cable insulation effectiveness and increasing the risk of operational failures or breakdowns [1,2].

Thermal stress is considered one of the primary stresses accelerating the ageing of extruded power cables [3]. The principal source of thermal stresses arises from the resistive heat of the heavily loaded cable core conductor. The resistive heat generated in the core conductor propagates throughout the cable insulation and might increase the insulation temperature beyond its designed limit. Furthermore, excessively high ambient temperature conditions can also contribute to the thermal ageing of cable insulation. In addition to the cable temperature itself, the thermal degradation of extruded power cables is closely related to their polymer structure and the effectiveness of antioxidants [4].

The estimation of a good electrical cable insulation condition is inherently associated with a heightened resistance to electric current flow. Insulation resistance (IR) testing is a widely acknowledged condition monitoring technique, demonstrating an ability to directly

infer the current state of cables [5]. Most research related to power cable ageing has placed a notable emphasis on the increase in electrical conductivity or the decrease in electrical resistivity for the insulation materials throughout the ageing processes [6–11]. Mecheri et al. delved into the impacts of prolonged thermal ageing on dielectric and mechanical properties of cross-linked polyethylene (XLPE) insulation of high voltage (HV) cables [7]. To ascertain the degree of the XLPE material deterioration resulting from thermal ageing and prevent potential failures, an extensive examination was conducted by encompassing volumetric resistivity assessments and additional condition monitoring evaluations on dumb-bell- and circular-shaped XLPE probes over a duration of 5000 h. The findings revealed a significant reduction in resistivity, amounting to several hundredfold, caused by the concurrent decrease in polymer viscosity which was considered to increase the mobility of charge carriers within XLPE. Nedjar [8] examined the influences of thermal ageing on the electrical characteristics of XLPE employed in HV cables, demonstrating that thermal ageing induced notable modifications in the electrical properties of the polymer. In particular, elevating the thermal ageing temperature leads to a faster reduction in resistivity, aligning with the principle outlined by the Arrhenius law. With the thermal ageing process going further, molecular bonds exhibited weakening, resulting in an augmentation of free volume. This phenomenon subsequently heightened the mobility of charge carriers, accompanied by a decline of volumetric resistivity. Mecheri et al. performed a comprehensive investigation into the impacts of thermal ageing conditions on the performance of XLPE for medium voltage (MV) 18/30 kV cables [9]. XLPE specimens of the same material were subjected to thermal stresses under a controlled environment facilitated by a forced air-circulating oven. The assessments on XLPE thermal degradation were carried out through the volumetric resistivity testing under a direct current (DC) voltage of 500 V at a measurement temperature of 85 °C. After 1350 h of thermal ageing at 90 °C, XLPE resistivity was observed to significantly decrease from around 700 TΩ·cm to 2.5 TΩ·cm. Discernible resistivity reductions were further pronounced at higher ageing temperatures of 135 °C and 150 °C, where the volumetric resistivity values declined to 0.46 TΩ·cm and 0.2 TΩ·cm, respectively, after 1350 h of thermal ageing.

Zhang et al. investigated the impacts of thermal ageing temperatures and durations on the DC electrical conductivity of XLPE insulation materials for HVDC cables by using Fourier transform infrared (FTIR) spectra [10]. The experimental findings and subsequent analysis revealed a sequential pattern in the DC electrical conductivity of thermally aged XLPE insulation, which initially declined below the level observed on unaged XLPE insulation and then exhibited a gradual increase over the entire ageing period due to the combined effects of thermal decomposition, post-crosslinking and the diffusion of low molecular weight substances. In addition, it was observed that higher thermal ageing temperatures induced more pronounced changes in the electrical conductivity of XLPE insulation. When subjected to the same ageing duration of 700 h, the variations of the DC electrical conductivity of XLPE insulation with ageing temperatures complied well with the Arrhenius equation. Kang and Kim performed a comprehensive assessment on IR properties of low voltage cables, subjecting them to external flame exposure, over-current conditions and accelerated degradation trials [11]. The results revealed a notable IR reduction from a peak of 7.5 TΩ to 0.008 TΩ during direct flame contact. However, it demonstrated a complete recovery to its initial state when cooling down to room temperature. In accelerated degradation experiments simulating 10 to 30 years of cable operation, no notable IR decline was observed at room temperature. Nevertheless, upon reaching an induced ageing equivalent to 40 years, a rapid IR reduction was observed at room temperature.

A significant challenge of comprehending the dielectric insulation condition lies in developing a quantitative approach to assessing insulation degradation over time. A dichotomy model was originally proposed by Chang et al. [12] to predict the IR of rectangular (unit cube) insulation bulk. It regards an entire insulation specimen cube as a combination of multiple small sub-cubes and divides them into degraded and non-degraded sub-cubes which possess disparate resistivity. The volume ratio of the two parts is estimated from

thermal ageing temperature and duration, based on which the positions of degraded sub-cubes within the specimen are randomly sampled to evaluate the overall IR. According to the original dichotomy model, the electrical resistance degradation trend of the XLPE material under thermal ageing can be classified into three phases, as shown in Figure 1 [12]:

- Phase 1: IR gradually decreases from an initial resistance R_0 since thermal ageing conditions are applied on insulation till a time t_s;
- Transition phase: IR significantly decreases within a short period from t_s to t_f due to the percolation phenomenon occurring in the insulation bulk;
- Phase 2: After t_f, IR gradually approaches toward a completely degraded resistance constant R_d.

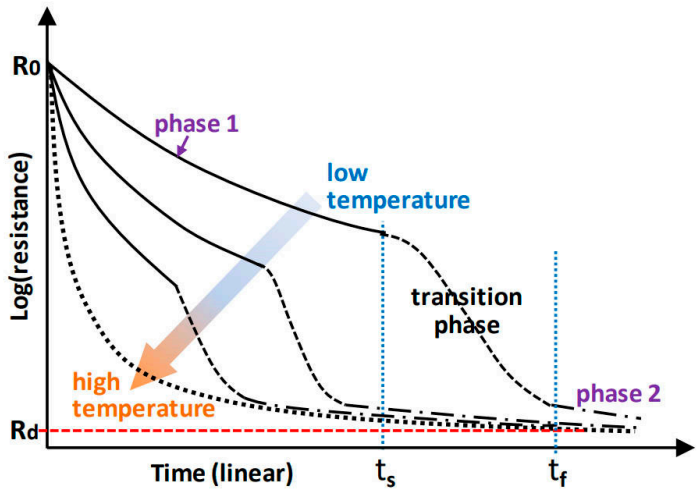

Figure 1. Temperature-dependent IR degradation of XLPE materials under thermal ageing [12].

Even though the original dichotomy model is able to describe the long-term decline of IR over thermal ageing time, it assumes that the insulation is uniform in ageing temperature and chooses the degraded sub-cubes in a random way. The contributions of this paper are to enhance the dichotomy model by simulating different degradation degrees between insulation layers under radial temperature gradients and additionally propose a discretization model that simulates the thermal degradation of individual insulation segments separately given a non-uniform temperature distribution. Furthermore, the developed IR degradation models adapt the original unit cube insulation model to a cylindrical insulation model in order to reflect the geometry of a practical cable insulation. In addition, the finite volume method (FVM) and artificial neural network (ANN) models are jointly employed to simulate the temperature distribution of cable insulation, which is then incorporated into the enhanced dichotomy model or the novel discretization model to evaluate IR degradation during Phase 1 in Figure 1. In order to perform a comparison not only between the dichotomy and discretization models but also between the uses of different temperature profiles, four IR degradation models are developed in this work:

- a dichotomy model with uniform temperature distribution;
- a dichotomy model with radial temperature gradients;
- a discretization model with uniform temperature distribution;
- a discretization model with non-uniform temperature distribution.

These models help investigate the influences of model methodologies and temperature profiles on the IR degradation simulation of power cables under thermal ageing. In addition, different segment sizes and degradation rates are applied to examine their effects on the IR degradation simulation.

The paper is structured as follows: Section 2 describes the IR degradation model development; Section 3 presents the application of the four IR degradation models with the temperature profile simulated under thermal ageing conditions; Section 4 discusses

the effects of segment sizes and degradation rates on IR simulation results; and Section 5 presents conclusions and recommendations for further work.

2. IR Degradation Models

Based on the discretization methodology [13], a sample of extruded power cable insulation can be conceptualized as a cylindrical volume made up of a substantial number of small segments, as illustrated in Figure 2a, where the inner radius, outer radius and length of the cable insulation model are denoted by x, X and L, respectively, all in meters. The position of the center of each segment is represented in a cylindrical coordinate system in the form of (x_i, φ_j, l_k), as shown in Figure 2b, where x_i (m), φ_j (arc degree) or l_k (m) denotes the position of a segment along the radial, angular or longitudinal dimension, respectively.

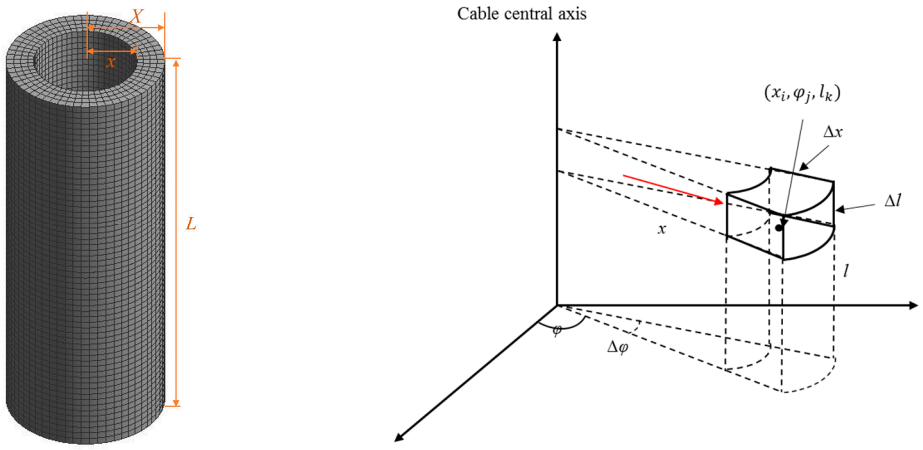

(**a**) (**b**)

Figure 2. (**a**) Model of cable insulation divided into multiple segments; and (**b**) shape and position of a segment in the cable insulation model, with a red arrow representing the direction of the current flowing through insulation.

Denoting radial, angular and longitudinal sizes of each segment by Δx, $\Delta\varphi$ and Δl, respectively, the resulting numbers of segments along radial, angular and longitudinal dimensions are equal to $M = (X - x)/\Delta x$, $N = 360^\circ/\Delta\varphi$ and $P = L/\Delta l$, respectively. The total number of segments in the cable insulation model then equals $N_t = M \times N \times P$.

The volume of a segment in the cable insulation model is dependent on its position along the radial axis. The segments located at outer insulation layers have larger volumes than those at inner insulation layers. The electrical resistance of any insulation material not only depends on its material resistivity (ρ in Ω-m) but also on shape and volume [14]. The integral formula of electrical resistance (R in Ω) for variable cross-section resistors with parallel curved terminals can be formulated by (1) [15]:

$$R = \frac{1}{A(l_1)} \int_{l_1}^{l_2} \frac{\rho(l)}{(1 + \kappa_{\uparrow}(l - l_1))(1 + \kappa_{\rightarrow}(l - l_1))} \tag{1}$$

where l_1 or l_2 is the arc-length parameter of each terminal measured through its normal surface ($l_2 > l_1$), $A(l_1)$ represents the cross-section area located at l_1 and $\rho(l)$ is the resistivity of the segment. The specific signed principal curvature values of $\kappa_{\uparrow}$ and $\kappa_{\rightarrow}$ for the cylindrical segment terminals are equal to 1 and 0, respectively.

It is assumed that the electric current flows through individual insulation segments along the radial axis with a uniform density (i.e., radially from the core conductor to any surrounding outer ground sheath), as indicated by the red arrow in Figure 2b. In addition, the material resistivity is assumed to be uniform within an individual insulation segment given its sufficiently small volume. For the insulation segment located at (x_i, φ_j, l_k) with

resistivity $\rho(x_i, \varphi_j, l_k)$, $(i = 1, 2, \ldots, M;\ j = 1, 2, \ldots, N;\ k = 1, 2, \ldots, P)$, based on (1), its resistance $R_e(x_i, \varphi_j, l_k)$ can be formulated by (2):

$$R_e(x_i,\ \varphi_j,\ l_k) = \frac{\rho(x_i,\ \varphi_j,\ l_k)}{\Delta\varphi\Delta l} \ln\left(\frac{x_i + \frac{\Delta x}{2}}{x_i - \frac{\Delta x}{2}}\right) \tag{2}$$

The resistances of all the insulation segments are converted into the total resistance of the power cable insulation based on the equivalent resistance model for a DC circuit. The series resistance of all the segments along an individual radial column at fixed angular and longitudinal locations is first estimated, making the insulation model have resistances of $N \times P$ columns. Then, the parallel resistance of all the columns within each individual plane at every fixed longitudinal location is calculated. Finally, the total resistance R_t of cable insulation is derived from the parallel connection of all the plane resistances. In other words, all the radial columns within the insulation are parallel connected. The total IR, R_t, is formulated by:

$$R_t = \frac{1}{\sum_{k=1}^{P}\sum_{j=1}^{N}\left(\frac{1}{\sum_{i=1}^{M} R_e(x_i,\varphi_j,l_k)}\right)} \tag{3}$$

The estimation of resistivity ρ for individual insulation segments by the four different IR models is detailed in the following subsections, respectively.

2.1. Dichotomy Model with Uniform Temperature Distribution

The dichotomy models categorize insulation segments into two types, virtually non-degraded and degraded segments, which are assumed to have resistivity values of ρ_0 and ρ_d, respectively. The value of ρ_0 is considered to be much greater than ρ_d. According to (2), the resistances of non-degraded and degraded segments (denoted by R_0 and R_d) are formulated by (4) and (5), respectively:

$$R_0(x_i,\ \varphi_j,\ l_k) = \frac{\rho_0}{\Delta\varphi\Delta l} \ln\left(\frac{x_i + \frac{\Delta x}{2}}{x_i - \frac{\Delta x}{2}}\right), \quad (x_i,\ \varphi_j,\ l_k) \neq (x_l,\ \varphi_m,\ l_n) \tag{4}$$

$$R_d(x_l,\ \varphi_m,\ l_n) = \frac{\rho_d}{\Delta\varphi\Delta l} \ln\left(\frac{x_l + \frac{\Delta x}{2}}{x_l - \frac{\Delta x}{2}}\right), \quad (x_i,\ \varphi_j,\ l_k) \neq (x_l,\ \varphi_m,\ l_n) \tag{5}$$

When the ageing temperature distribution is uniform within the cable insulation and also within individual segments, the number N_d of degraded segments to be randomly sampled within the insulation model depends on the total number N_t of segments and the degradation volume ratio V_d, i.e., $N_d = N_t \times V_d$. Assuming that the degradation rate does not change with ageing time t, the value of V_d can be determined based on the cumulative distribution function (CDF) of an exponential distribution in terms of t [16]:

$$V_d(t) = 1 - e^{-\lambda(T)\cdot t} \tag{6}$$

where the degradation rate $\lambda(T)$ (in 1/h) of insulation material is a function of the ageing temperature T (in K) depending on material properties and generally obtained from the IR decay tendency rather than the measurement of chemical reaction. Considering in this work, and for this model, that the degradation of cable insulation is thermally activated, $\lambda(T)$ is presumed to follow the Arrhenius model [16] as formulated by (7):

$$\lambda(T) = \lambda_0 \cdot e^{\left(\frac{-E_a}{k_B \cdot T}\right)} \tag{7}$$

where λ_0 is a constant (1/h) obtained from experimental data, k_B is the Boltzmann constant of 1.38×10^{-23} J/K and E_a is the IR thermal degradation activation energy (J) of insulation

material. Then, the degradation volume ratio and the number of degraded segments within the insulation can be calculated by (8) and (9), respectively:

$$V_d(t,T) = 1 - e^{-(\lambda_0 \cdot \exp(\frac{-E_a}{k_B \cdot T})) \cdot t} \quad (8)$$

$$N_d(t,T) = N_T \cdot V_d(t,T) \quad (9)$$

Since this model assumes a uniform temperature distribution for cable insulation, the locations of the degraded segments accompanying their resistivity ρ_d are randomly and uniformly sampled within the insulation. A flowchart showing the IR estimation by the dichotomy model with uniform temperature is presented in Figure 3.

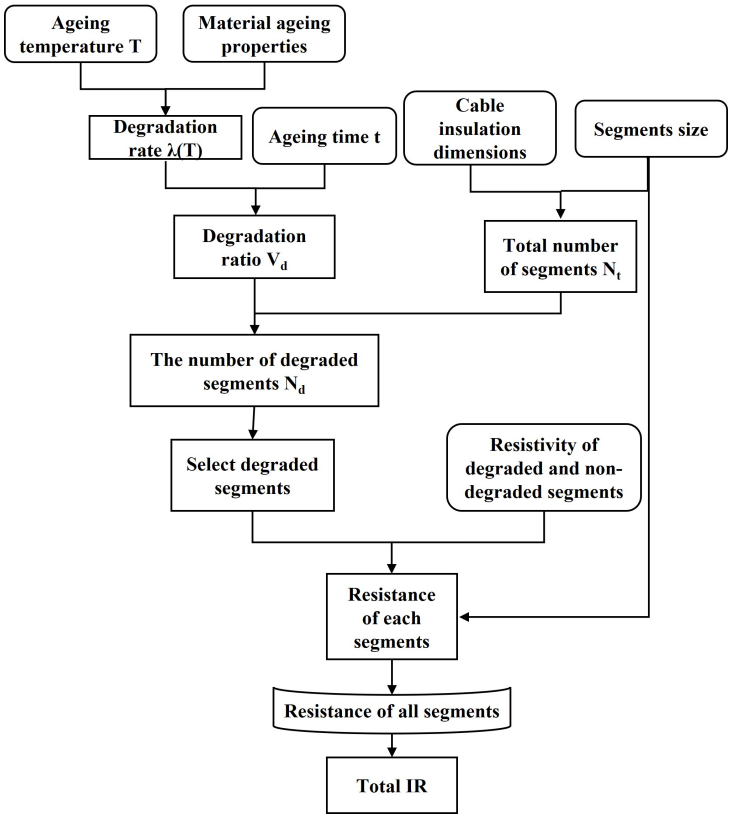

Figure 3. IR estimation process of a dichotomy model with uniform temperature.

2.2. Dichotomy Model with Radial Temperature Gradients

When considering the temperature gradients along the cable radius created by the propagation of resistive heat from the core conductors through insulation layers, outer insulation layers closer to the ambient environment and further away from the core conductors have lower temperatures than inner insulation layers, as shown in Figure 4. The introduction of insulation temperature gradients into the dichotomy model will produce more reliable IR results when power cables are carrying currents.

According to the Arrhenius model [17], the radial temperature gradients will result in inner insulation layers having higher degradation volume ratios than outer insulation layers. Given that the temperature of the *i*th insulation layer along the radial axis is fixed at T_i, its degradation volume ratio $V_{d(i)}$ and the number $N_{d(i)}$ of degraded segments at ageing time t can be calculated by (10) and (11), respectively:

$$V_{d(i)} = 1 - e^{-(\lambda_0 \cdot \exp(\frac{-E_a}{k_B \cdot T_i})) \cdot t} \quad (10)$$

$$N_{d(i)} = N_{t(i)} \cdot V_{d(i)} \quad (11)$$

where $N_{t(i)}$ is the total number of segments in the i^{th} layer equalling $(N \times P)$. Since the model assumes a constant temperature for each individual layer, the locations of the $N_{d(i)}$ virtually degraded segments accompanying their resistivity ρ_d within each layer are randomly and uniformly selected for that layer. The IR estimation process of the dichotomy model with radial temperature gradients is shown in Figure 5.

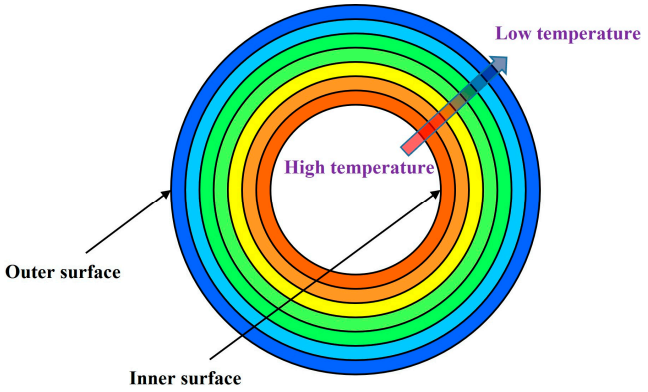

Figure 4. Schematic of insulation temperature gradients along cable radius.

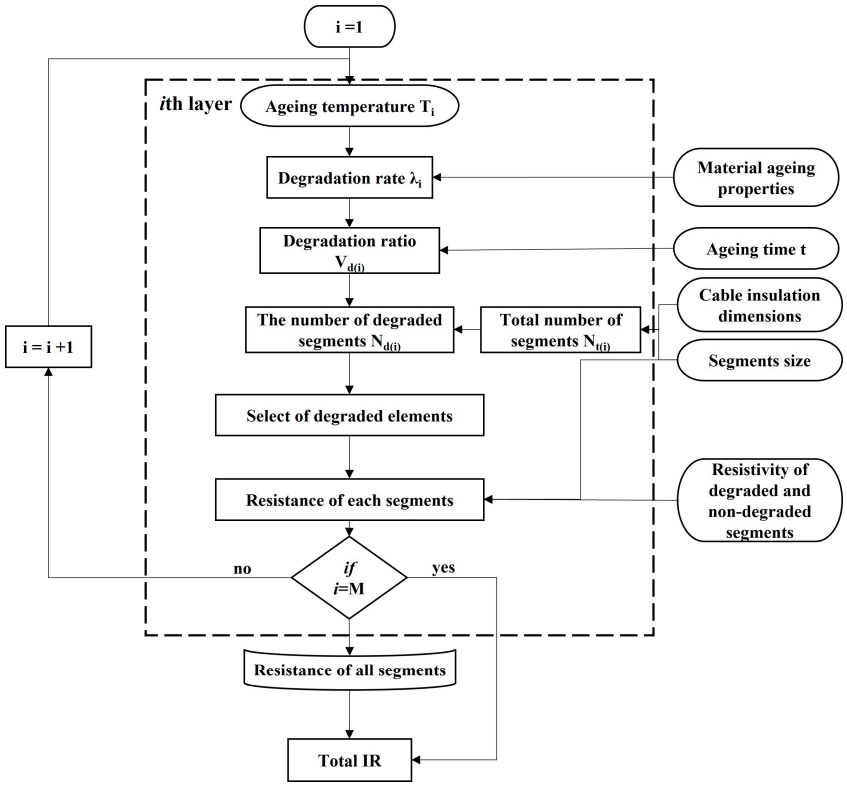

Figure 5. IR estimation process of a dichotomy model with radial temperature gradients.

2.3. Discretization Model with Uniform Temperature Distribution

Compared with the dichotomy models which differentiate the segment resistivity between non-degraded ρ_0 and fully degraded ρ_d only, the discretization models proposed here simulate the gradual resistivity degradation of individual segments separately by a function of thermal ageing time t and ageing temperature T. Assuming that insulation segments have consistent temperature, their resistivity is modelled to exponentially decline with t at the same degradation rate $\lambda(T)$:

$$\rho(t, T) = \rho_0 \cdot e^{-\lambda(T) \cdot t} \quad (12)$$

where $\lambda(T)$ complies with the Arrhenius model as formulated by (7). The resistance of each segment is then calculated by (13) based on its location along the radial axis, segment sizes and $\rho(t, T)$. The process of IR estimation by the discretization model with uniform temperature is described in Figure 6.

$$R_e(x_i,\ \varphi_j,\ l_k, t) = \frac{\rho(t,T)}{\Delta\varphi\Delta l}\ln\left(\frac{x_i + \frac{\Delta x}{2}}{x_i - \frac{\Delta x}{2}}\right) \tag{13}$$

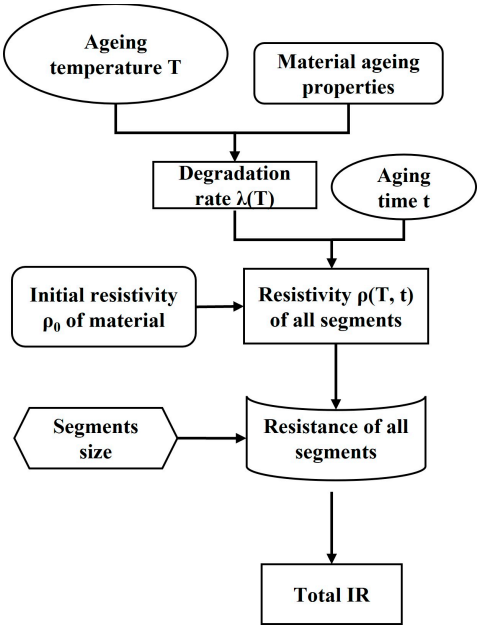

Figure 6. IR estimation process of a discretization model with uniform temperature.

2.4. Discretization Model with Non-Uniform Temperature Distribution

As it was noted in Section 2.2, the temperature distribution of cable insulation is generally non-uniform along its radial axis. The cable temperature will also vary longitudinally along the cable especially when it spans a long distance with various ambient environment such as solar irradiation, wind velocity and soil moisture content [18]. The non-uniform temperature along multiple dimensions will cause degradation rates to vary with the positions within cable insulation. Given the temperature T' of a particular insulation segment locating at (r_i, φ_j, l_k), its resistivity and resulting resistance at t can be calculated by (14) and (15), respectively. A flowchart describing the IR estimation by the discretization model with a non-uniform temperature distribution is shown in Figure 7.

$$\rho(x_i, \varphi_j, l_k, t, T') = \rho_0 \cdot e^{-\lambda(x_i, \varphi_j, l_k, T')\cdot t} \tag{14}$$

$$R_e(r_i, \varphi_j, l_k, t, T') = \frac{\rho(x_i, \varphi_j, l_k, t, T')}{\Delta\varphi\Delta l}\ln\left(\frac{x_i + \frac{\Delta x}{2}}{x_i - \frac{\Delta x}{2}}\right) \tag{15}$$

It is noted that the flow charts in Figures 3 and 5–7 are applied at each ageing time step to estimate the IR value after a particular thermal ageing period. For dichotomy models, the number of degraded segments is first determined at each individual ageing time step. Then, the locations of the degraded segments selected in the previous time step are kept, while new degraded segments are uniformly and randomly sampled from the locations of the remaining non-degraded segments. For discretization models, the resistivity of insulation segments is updated at every ageing time step.

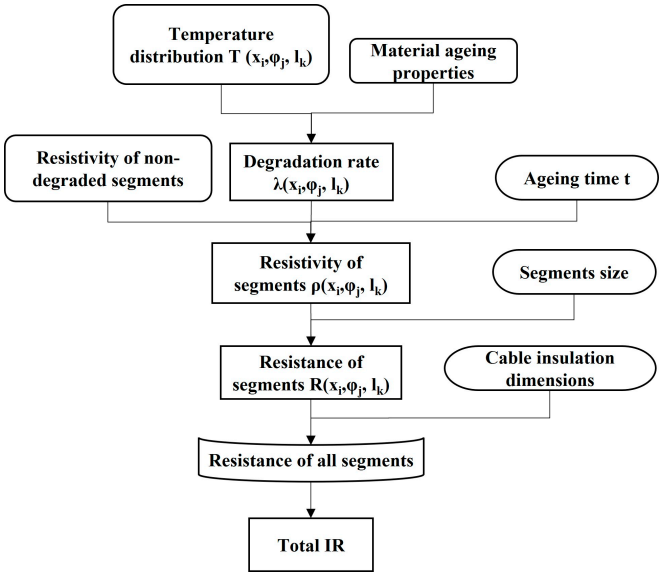

Figure 7. IR estimation process of a discretization model with non-uniform temperature.

3. Application of IR Degradation Models

3.1. Degradation Model Parameters Estimation

The parameters of the four IR degradation models are estimated based on the experimental data of XLPE insulation referenced from the research of Mecheri et al. [7] where XLPE insulation samples were thermally aged at four different temperature levels of 80 °C, 100 °C, 120 °C and 140 °C (i.e., 353.15 K, 373.15 K, 393.15 K and 413.15 K, respectively). The XLPE sample resistivity was measured through a megohmmeter by applying a DC voltage of 500 V for a duration of 10 min. Figure 8 shows the XLPE resistivity measurements under different thermal ageing temperatures, which generally declined with the thermal ageing time, with the pattern being affected by the ageing temperature.

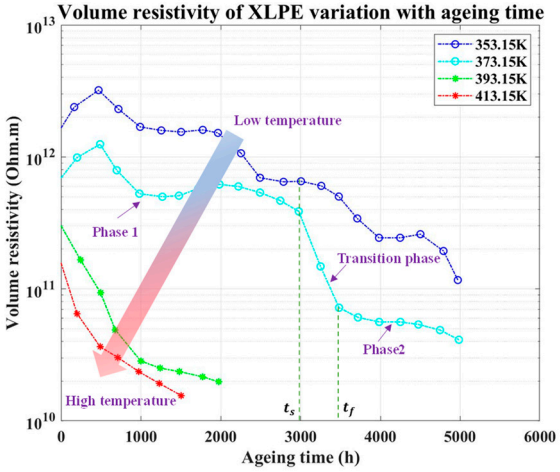

Figure 8. Volume resistivity (Ω·m) of XLPE insulation varying with ageing time and temperature [7].

To explore the dependency of the IR degradation model parameters on temperature, the values of λ, ρ_0 and ρ_d for each temperature level are first determined from the corresponding XLPE resistivity measurements in Figure 8. The software Origin 2022 is used here to estimate λ, ρ_0 and ρ_d in (12) by fitting the decay of XLPE resistivity over Phase 1 of the thermal ageing process prior to the occurrence of a percolation phenomenon in the transition phase. The results of λ, ρ_0 and ρ_d estimated for the four ageing temperature levels are listed in Table 1. Taking the natural logarithm of the Arrhenius model which links λ to T via the IR thermal ageing activation energy E_a, as formulated by (16), the parameters

λ_0 and E_a are computed by fitting (16) to the degradation rate estimates in Table 1, as shown in Figure 9a, which equal 1.82×10^6 (1/h) and 64 kJ, respectively. Figure 9b,c show the linear fitting of ρ_0 and ρ_d against temperatures, which is used here to approximately describe the dependencies of ρ_0 and ρ_d on T, as formulated by (17) and (18), respectively. The statistics of the linear fitting of $\ln(\lambda)$, ρ_0 and ρ_d against T are listed in Table 2. While the linear fitting of $\ln(\lambda)$ and ρ_0 achieves an R-squared of about 0.9, the R-squared for the linear fitting of ρ_d is 0.54 only. The fitting could be improved by using a function with a higher degree of freedom, though this might cause an over-fitting problem. The data obtained from more XLPE samples and more temperature levels can be considered for a better fitting of the temperature-dependent variables.

$$\ln(\lambda) = \left(-\frac{E_a}{k_B}\right)\frac{1}{T} + \ln(\lambda_0) \tag{16}$$

$$\rho_0 = (-3.0475 \times T + 1255.52) \times 10^{10} \tag{17}$$

$$\rho_d = (0.0126 \times T - 3.4677) \times 10^{10} \tag{18}$$

Table 1. Degradation rates, non-degraded and degraded resistivity values obtained from resistivity measurements of XLPE insulation samples at different thermal ageing temperatures.

Temperature (K)	Degradation Rate λ (1/h)	ρ_0 (Ω-m)	ρ_d (Ω-m)
353.15	8.5×10^{-4}	2.0×10^{12}	1.0×10^{10}
373.15	1.0×10^{-3}	1.0×10^{12}	1.0×10^{10}
393.15	9.0×10^{-3}	3.2×10^{11}	1.9×10^{10}
413.15	1.4×10^{-2}	1.95×10^{11}	1.54×10^{10}

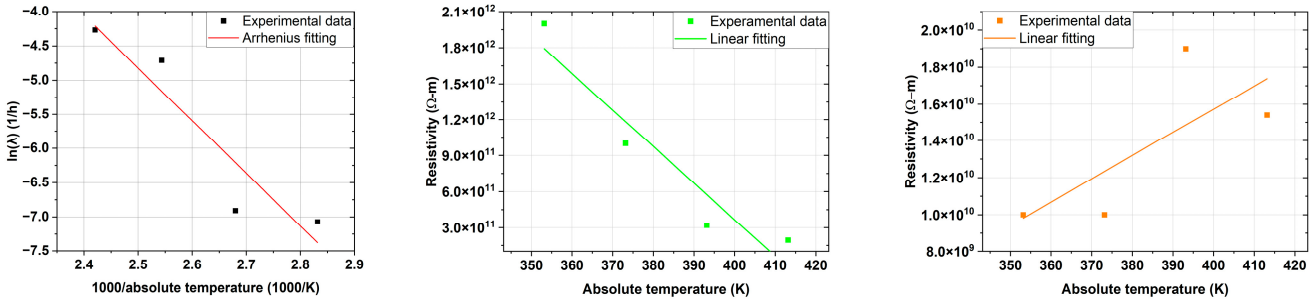

(**a**) (**b**) (**c**)

Figure 9. (**a**) The Arrhenius plot of the natural logarithm of degradation rate against the inverse of absolute temperature; and the linear fitting of (**b**) non-degraded resistivity and (**c**) degraded resistivity against absolute temperature for XLPE insulation samples.

Table 2. The statistics of linear fitting of the natural logarithm of degradation rate, non-degraded and degraded resistivity against absolute temperature for XLPE insulation samples.

Fitting Statistics		$\ln(\lambda)$	ρ_0	ρ_d
Intercept	Value	14.4153	1255.5200×10^{10}	-3.4677×10^{10}
	Std. Err.	5.3673	267.4020×10^{10}	3.1279×10^{10}
	t-Value	2.6858	4.6953	−1.1086
Slope	Value	−7.6959	-3.0475×10^{10}	0.0126×10^{10}
	Std. Err.	2.0460	0.6967×10^{10}	0.0081×10^{10}
	t-Value	−3.7615	−4.3741	1.5460
Residual Sum of Squares		0.7874	1941.6750×10^{20}	0.2657×10^{20}
R-squared		0.8762	0.9054	0.5444

3.2. Experiment Design and Temperature Simulation

The model parameters estimated in Section 3.1 are applied here to simulate the IR of an XLPE insulation sample with inner radius x of 0.0075 m, and outer radius X of 0.0115 m (i.e., a 0.004 m insulation thickness). Long term laboratory experiments have been undertaken on the surface temperature measurements along a number of 3.2 m LSXHIOE 1 × 185/35, 6.35/11 kV XLPE-insulated power cable samples in a temperature ageing enclosure running increased currents to produce cable surface temperatures of approximately 100 °C [19]. The surface temperature distribution across the length of the cables was measured using five type T temperature sensors as depicted in Figure 10. An FVM simulation model was also implemented to replicate the measurements to a reasonable degree of accuracy, as shown in Figure 11. The details are too extensive to reproduce here, but as an example an outer temperature of 100 °C was simulated in order to produce an understanding of the inner temperature distribution across the cable insulation. The example is displayed in Figure 12 which shows the temperature profile at one cross section of the cable with natural convection air flow in the ageing chamber. The purpose of this is to demonstrate the power of the FVM model in being able to provide data that can be fed to an ANN model to estimate the temperature at any position within the insulation. Different FVM simulations can be applied for different physical geometries and scenarios and this is simply one scenario to demonstrate the principles of the methodology. For the details of FVM simulation and the coefficients of cable layer and air properties, the reader is referred to [20] and [21–24], respectively.

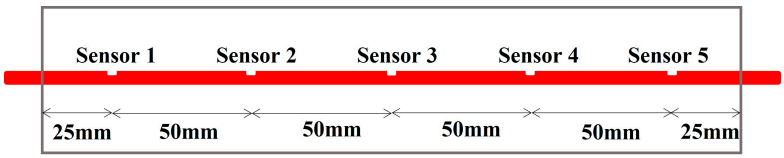

Figure 10. Positions of type T thermocouples placed along the cable sample surface.

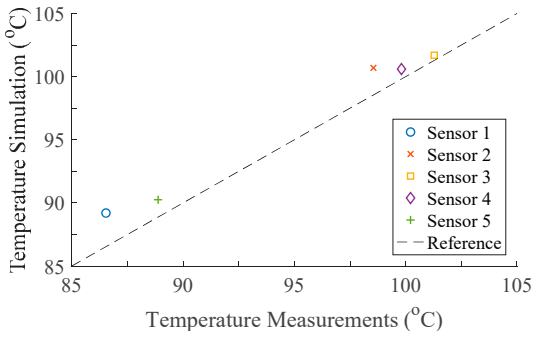

Figure 11. Measurements and simulation of cable surface temperatures (°C) at the sensor positions.

In order for the resolution of the FVM-based temperature simulation to meet the sizes of insulation segments, the FVM-based temperature simulation results were used to train the ANN model [25] which then interpolated the temperature for all the segments. The MATLAB neural network toolbox [26] was employed to construct the ANN model which was trained based on 70% of the temperature data obtained from the FVM simulation. An amount of 15% of the temperature data was designated for validation, and the remaining 15% was used for testing. The ANN models underwent training for a total of 1000 iterations, with a Pearson correlation coefficient of over 0.99 indicating an excellent performance of the ANN model. The temperature distributions estimated by the ANN model for the entire cable insulation and a selected 1 m insulation section starting from the middle of the cable sample are shown in Figures 13a and 13b, respectively. Higher temperatures generally occur at the segments closer to core conductors and/or the centre of the ageing chamber.

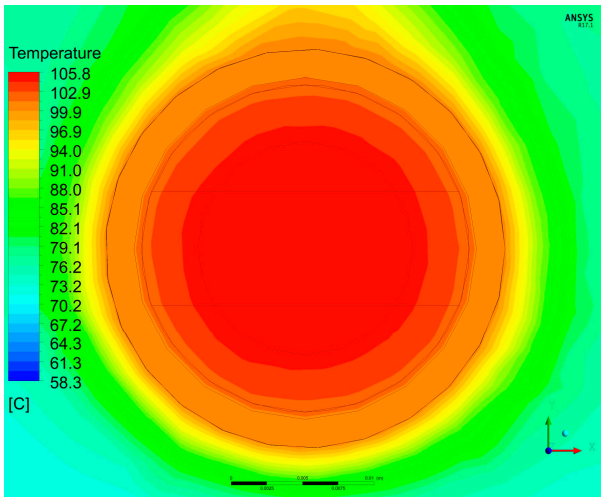

Figure 12. Example temperature profile simulation (°C) across one cross section of the cable sample.

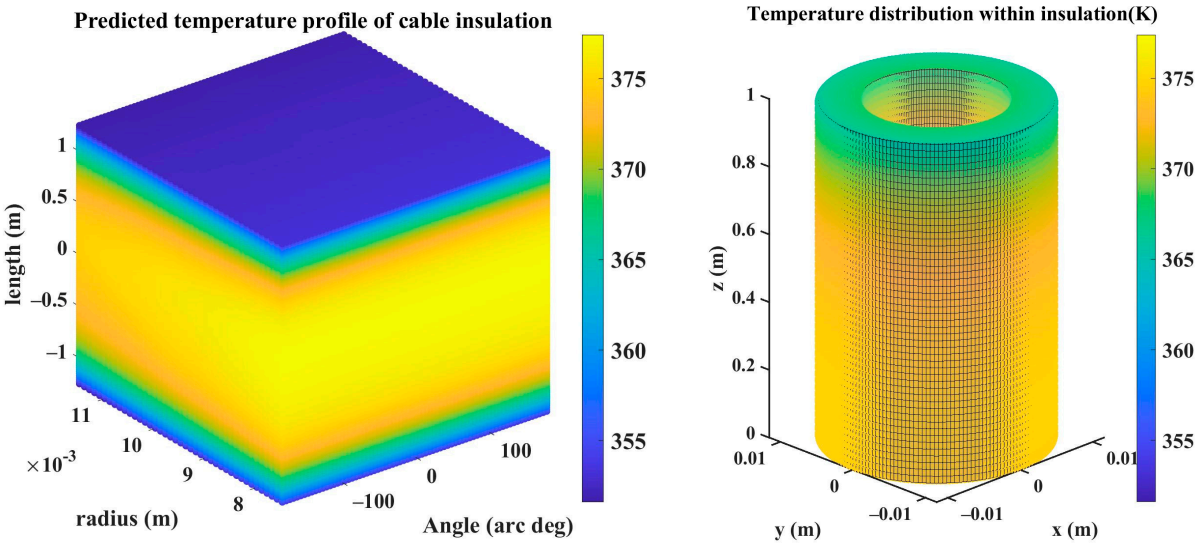

(**a**) (**b**)

Figure 13. Example temperature profiles (K) of (**a**) the entire cable insulation and (**b**) the selected 1 m insulation section in cylindrical coordinate system.

It is noted that the insulation temperature simulation performed by the FVM depicts the temperature profiles across insulation in the thermal ageing experiment and does not reflect the local temperature elevation in partial discharge events or a highly non-uniform temperature profile in the case of a complex ambient environment. While the FVM-based simulation shows its capability of replicating the temperature profiles in the experimental environment, the FVM can be enhanced to cope with the heat exchange of cables with the surrounding environment and reflect the effects of partial discharges on local temperature under practical operation, providing reliable insulation temperature profiles for thermal degradation assessment in practice. In addition, the existence of local temperature variations means that the dichotomy models which assume a uniform temperature distribution across the entire insulation (layer) are not applicable. In such cases, the discretization models can be employed to simulate the thermal degradation of individual insulation segments under a highly non-uniform temperature distribution.

3.3. IR Degradation Simulation Results

The 1 m cable insulation sample with constant diameters across its length, as shown in Figure 13b, is employed here to compare the performance of the four IR degradation models and simplify the conditions for IR simulation. Given the four IR degradation models considering temperature information in different ways, the hotspot temperature of 377.26 K within the entire insulation is applied to the dichotomy or discretization model with uniform temperature, and the discretization model with non-uniform temperature uses the exact insulation temperature profile. The dichotomy model with radial temperature gradients divides the insulation sample into 10 layers along the radial dimension. Table 3 lists the hotspot temperature adopted for each layer and related degradation rate which decreases from the innermost layer #1 to the outermost layers #10. As it was noted in Sections 2.1 and 2.2, the degraded insulation segments are selected by the dichotomy models in a random way. To that end, the IR simulation of the dichotomy models is performed 50 times to ensure reliability. The 50 potential IR estimates at each thermal ageing time step are found to have a negligible standard deviation which is smaller than 0.1%. Therefore, the one-time IR calculation results of the dichotomy models will be presented in this work.

Table 3. Hotspot temperatures and associated degradation rates of 10 insulation layers in the dichotomy model with radial temperature gradients.

Layer No.	Absolute Temperature (K)	Degradation Rate (1/h)
1	377.26	0.002505
2	376.96	0.002464
3	376.66	0.002424
4	376.36	0.002385
5	376.07	0.002348
6	375.86	0.002321
7	375.59	0.002287
8	375.33	0.002256
9	375.10	0.002227
10	374.82	0.002192

3.3.1. Initial Resistance Distributions

The initial resistances of insulation segments estimated by the four IR degradation models are shown in Figure 14, respectively. In the main, the segments at inner insulation layers which have relatively smaller volumes show higher resistances than those at outer layers. Since the (non-degraded) segment resistivity at the start of the thermal ageing process depends on segment temperature only, the dichotomy and discretization models which assume uniform temperature produce the same initial resistance distributions (see Figure 14a,c) which lead to a total IR of 94.6 GΩ. When the radial temperature gradients are introduced into the dichotomy model, the segments of outer layers with lower temperature will have higher resistivity than those that are assumed to be subjected to the hotspot temperature of the entire insulation. Therefore, the dichotomy model with radial temperature gradients produces relatively higher initial resistances for segments at outer layers than the model with uniform temperature (see Figure 14a,b). This results in a higher total IR equalling around 97.18 GΩ. When the full insulation temperature profile is introduced into the discretization model, the segment resistance variations with the position-dependent temperatures are simulated along longitudinal and radial dimensions (see Figure 14d). The total IR estimated by the discretization model at the start of the thermal ageing process is around 101.32 GΩ.

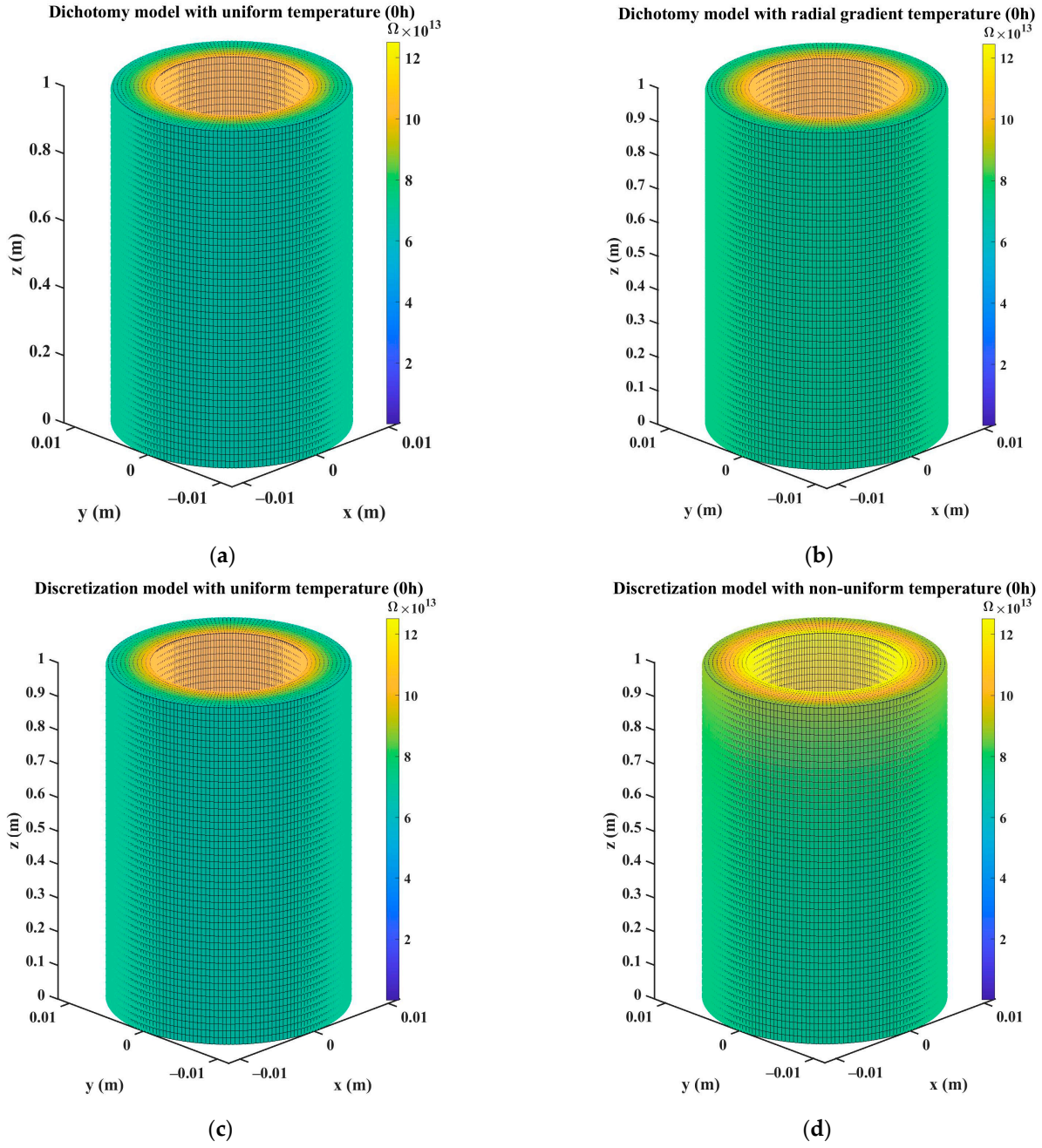

Figure 14. The segment resistances (Ω) of cable insulation at 0 h estimated by (**a**) dichotomy model with uniform temperature; (**b**) dichotomy model with radial temperature gradients; (**c**) discretization model with uniform temperature; and (**d**) discretization model with non-uniform temperature.

3.3.2. Resistance Distributions after 100 h and 300 h Thermal Ageing

Figures 15 and 16 compare the segment resistance distributions of the insulation sample modelled by the four IR degradation models for thermal ageing durations of 100 h and 300 h. Compared with the dichotomy models which assign low resistivity ρ_d to the random samples of fully degraded segments, the discretization models are shown to describe the gradual resistance degradation of individual insulation segments separately. Table 4 tabulates the degradation volume ratio and the resulting number of degraded segments that are randomly sampled for each insulation layer by the dichotomy model with radial temperature gradients. The degradation volume ratio determined from the temperature-based degradation rate not only increases with layer temperature but also with the thermal ageing duration, which is reflected in the increasing number of degraded

segment samples (see Figures 15b and 16b). Since the dichotomy model with uniform temperature uses the hotspot temperature of the entire insulation, the number of degraded segment samples at the outermost layer in Figure 15a is greater than in Figure 15b which is simulated with the radial temperature gradients. In addition, the inclusion of the full insulation temperature profile allows the discretization model to describe the dependency of individual segment degradation on local temperatures which vary along both radial and longitudinal dimensions, as shown in Figures 15d and 16d.

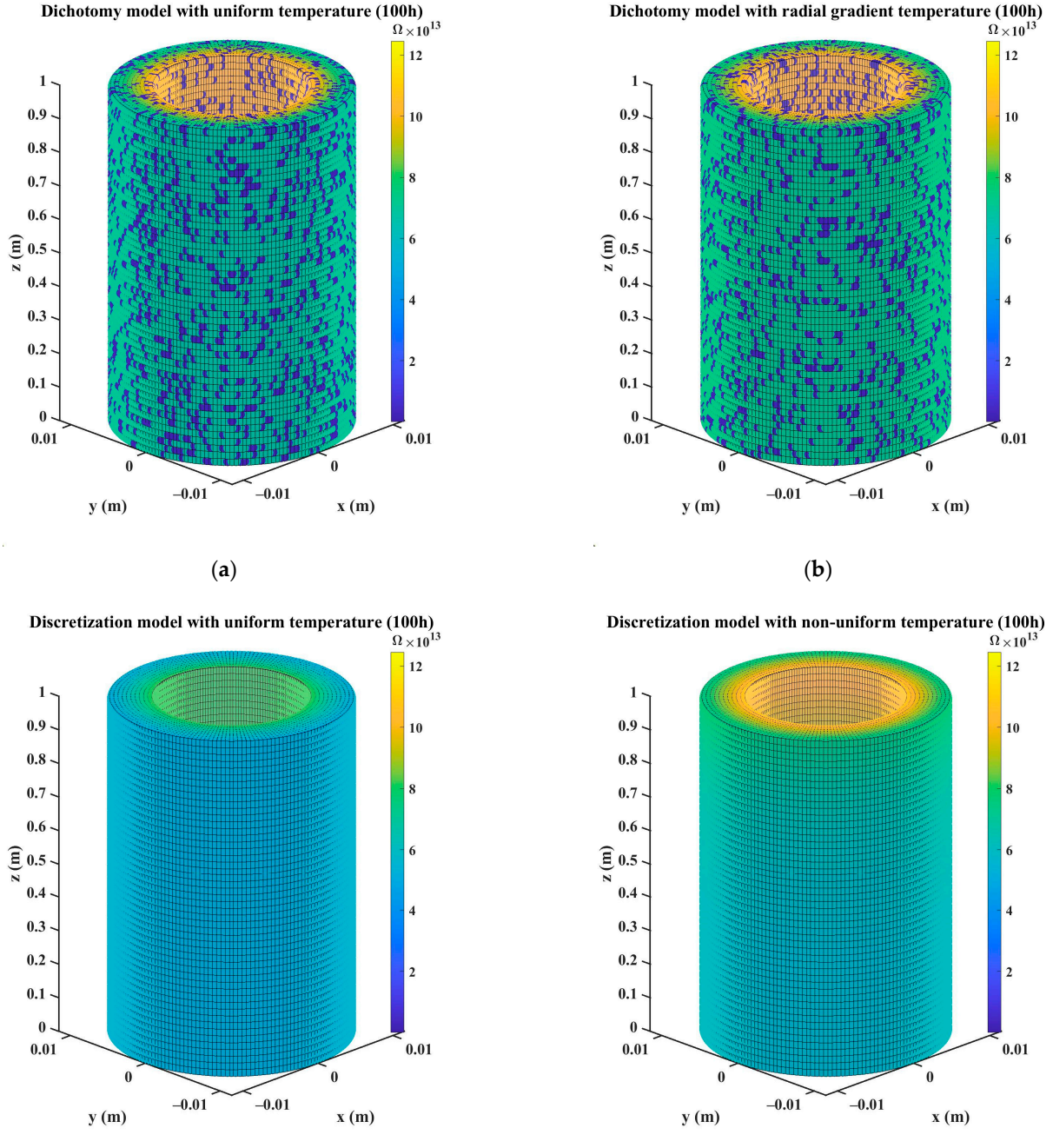

Figure 15. The segment resistances (Ω) of cable insulation at 100 h of thermal ageing estimated by (**a**) Dichotomy model with uniform temperature; (**b**) dichotomy model with radial temperature gradients; (**c**) discretization model with uniform temperature; and (**d**) discretization model with non-uniform temperature.

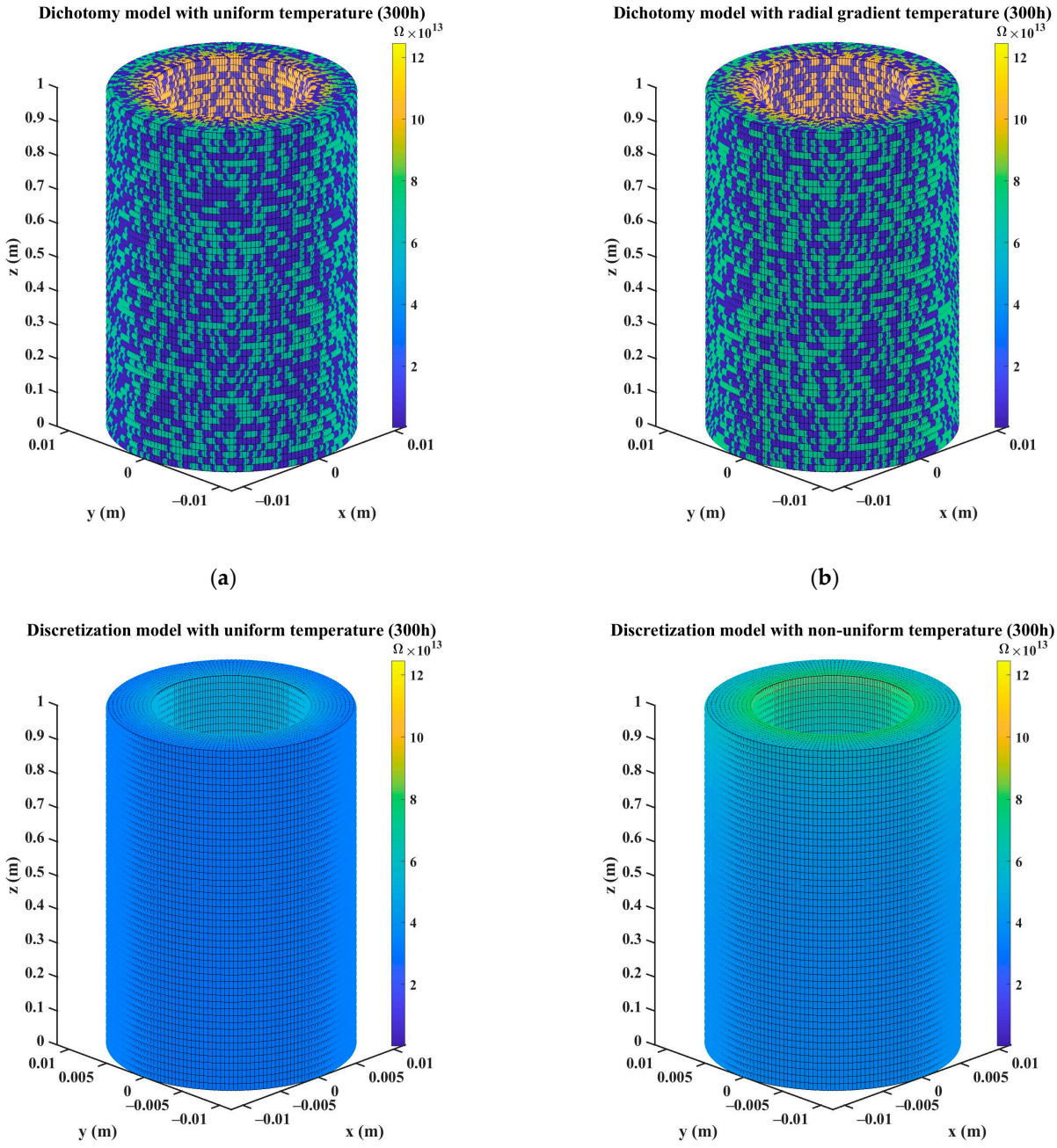

Figure 16. The segment resistances (Ω) of cable insulation at 300 h of thermal ageing estimated by (**a**) Dichotomy model with uniform temperature; (**b**) dichotomy model with radial temperature gradients; (**c**) discretization model with uniform temperature; and (**d**) discretization model with non-uniform temperature.

Table 4. Degradation volume ratios and numbers of degraded segments estimated for 10 insulation layers by the dichotomy model with radial temperature gradients after 100 h and 300 h of thermal ageing.

Layer	Thermal Ageing for 100 h		Thermal Ageing for 300 h	
	Degradation Ratio	Number of Degraded Segments	Degradation Volume Ratio	Number of Degraded Segments
1	22.158%	1994	52.833%	4755
2	21.836%	1965	52.245%	4702

Table 4. *Cont.*

Layer	Thermal Ageing for 100 h		Thermal Ageing for 300 h	
	Degradation Ratio	Number of Degraded Segments	Degradation Volume Ratio	Number of Degraded Segments
3	21.526%	1937	51.674%	4651
4	21.220%	1910	51.106%	4600
5	20.927%	1883	50.559%	4550
6	20.715%	1864	50.161%	4514
7	20.443%	1840	49.645%	4468
8	20.194%	1817	49.171%	4425
9	19.964%	1797	48.731%	4386
10	19.687%	1772	48.197%	4338

3.3.3. IR Degradation Curves in Short Term of Thermal Ageing

To examine the impacts of model assumptions on IR degradation simulation, the IR degradation curves generated by the four models over the initial short term (0–300 h) of thermal ageing are compared in Figure 17. Compared with the dichotomy model which uses the hotspot temperature of the entire insulation, the adoption of hotspot temperature for each of the 10 insulation layers under radial temperature gradients reduces the degradation rates and numbers of degraded segments at outer layers. This not only produces relatively greater IR simulation results but also slightly reduces the speed of the simulated IR degradation. In addition, different IR simulation results between dichotomy and discretization models which use the same uniform temperature reveal the inherent differences between the two models. The discretization model simulates the gradual IR degradation of individual segments separately, while the dichotomy model assesses the overall degradation condition of the insulation sample through a degradation volume ratio based on which the fully degraded segments are randomly located within the insulation sample. With the degradation volume ratio increasing over the thermal ageing process, the radial column consisting of series connected segments along the radial dimension becomes more likely to have multiple degraded segments, which largely reduces the column resistance and causes more degradation in the total IR. Therefore, the random selection of degraded segments by the dichotomy model leads to lower IR values than the discretization model, as shown in Figure 17. Furthermore, the discretization model with non-uniform temperature distribution is shown to generate the highest IR estimates throughout the duration of interest due to the use of a detailed insulation temperature profile instead of the hotspot temperature(s) of cable insulation.

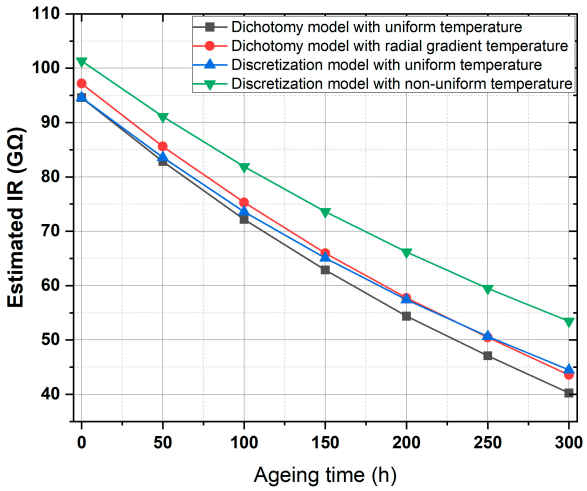

Figure 17. IR degradation curves (GΩ) estimated by different models within 300 h of thermal ageing.

4. Sensitivity Analysis

4.1. Influence of Segment Size

To examine the influence of the segment size adopted for the IR degradation simulation, the IR simulation results of the four IR models are simulated based on four different segments sizes, respectively, as listed in Table 5 where the size #2 is different from the size #1, #3 or #4 along the radial, longitudinal or angular dimension, respectively. The material properties and related parameters are the same as those that were employed in Section 3. To explore the IR degradation trend over a longer thermal ageing period, the IR results are simulated at every 50 h during 2000 h of thermal ageing, as shown in Figure 18.

Table 5. Insulation segment sizes and resulting numbers of segments for comparison.

Size Index	Δx (m)	Δφ (°)	Δl (m)	M	N	P	N_t
1	2×10^{-4}	2	0.02	20	180	50	1.8×10^5
2	1×10^{-4}	2	0.02	40	180	50	3.6×10^5
3	1×10^{-4}	2	0.01	40	180	100	7.2×10^5
4	1×10^{-4}	1	0.02	40	360	50	7.2×10^5

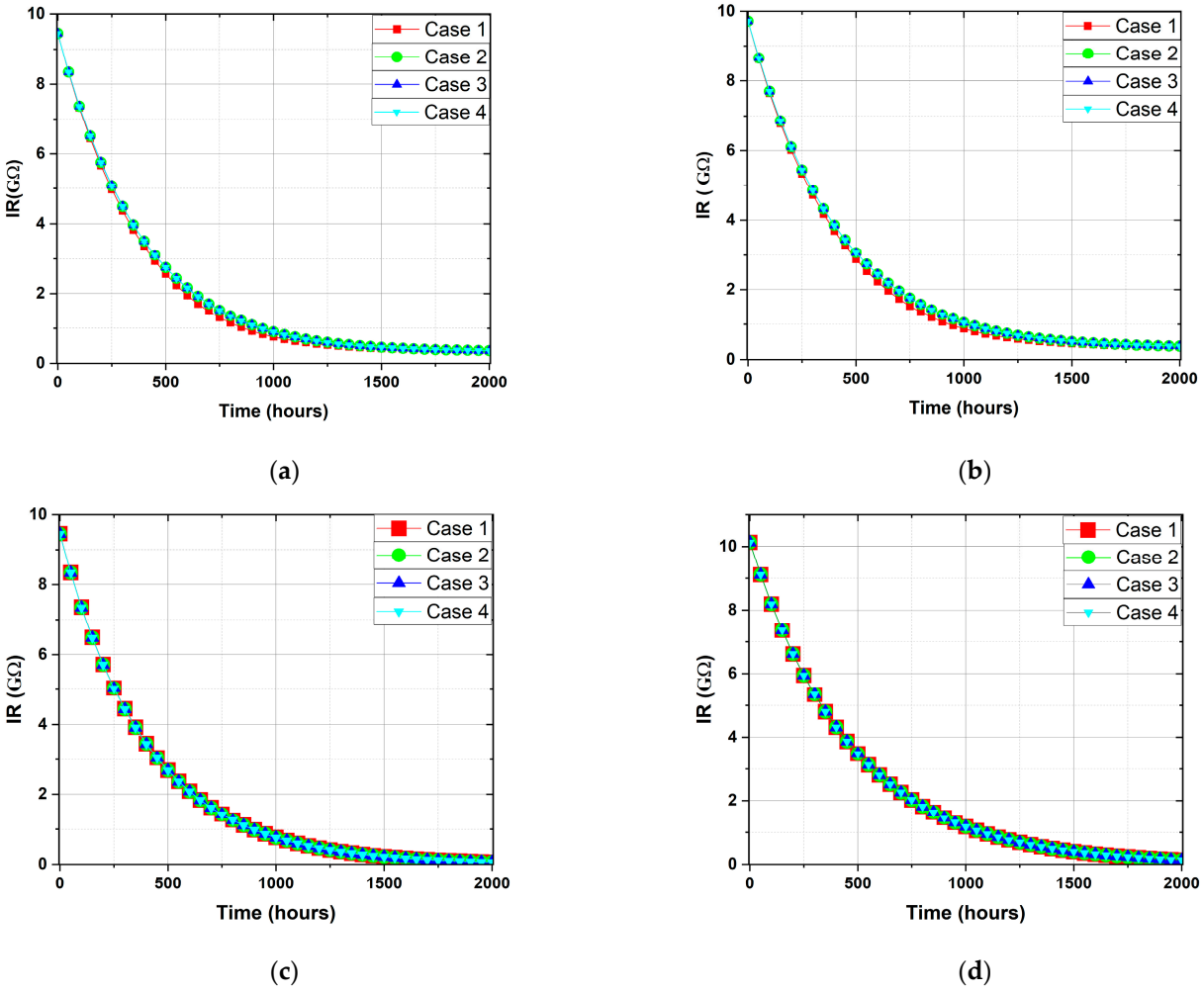

Figure 18. IR degradation trends (Ω) over 2000 h of thermal ageing simulated based on different segment sizes by (**a**) dichotomy model with uniform temperature; (**b**) dichotomy model with radial temperature gradients; (**c**) discretization model with uniform temperature; and (**d**) discretization model with non-uniform temperature.

Figure 18a,b show that the adoption of sizes #2, #3 and #4 in the dichotomy models almost produces the same IR results, meaning that the segment size change along the angular or longitudinal dimension examined in this work has negligible impacts on the IR simulation. When the size #1 is used by the dichotomy models, a degraded segment with a radial size $\Delta x = 0.2$ mm can be regarded as two degraded segments of $\Delta x = 0.1$ mm that are series connected in a column along the radial dimension. This increases the probability of a single radial column having more degraded parts and thus reducing the total IR. Therefore, compared with the sizes #2, #3 and #4 of $\Delta x = 0.1$ mm, the size #1 of $\Delta x = 0.2$ mm results in the dichotomy models producing slightly lower IR values, especially during 200–1200 h of thermal ageing. When the thermal ageing process approaches 2000 h, the effect of Δx on IR simulation becomes negligible due to a sufficient degradation volume ratio which makes the two different Δx values result in similar degradation parts of single radial columns. For the discretization models which simulate the individual segment degradation rather than rely on the random selection of fully degraded segments, the use of the four different segment sizes produces very similar IR results, as shown in Figure 18c,d. This illustrates that the segment size variations assessed in this work have little impact on the IR simulation of discretization models.

4.2. Influence of Degradation Rate

The degradation rates employed in the simulation above are determined through the Arrhenius fitting of experimental data sourced from Mecheri et al. [7]. Considering the possible inherent uncertainties, a percentage error of $\pm 10\%$ is introduced in the degradation rate, denoted by 0.9λ and 1.1λ. With other model parameters remaining fixed, the IR degradation trends simulated by the four models using the smaller segment size #3 combined with the three degradation rates are compared in Figure 19a–d, respectively.

Even though the uncertainties of degradation rates do not affect the IR degradation pattern, it is estimated that the IR percentage errors are less sensitive to the λ error of +10% and vary with thermal ageing time in different ways between the dichotomy and discretization models. The IR percentage error amplitudes of dichotomy models increase to a maximum of about 22% for 0.9λ or 16% for 1.1λ at around 900–1000 h and then relatively slowly drop with the ageing time going further. This might be because the dichotomy models randomly assign a constant fully degraded resistivity to insulation segments based on the number of degraded segments jointly determined by the degradation rate and ageing time. The variation in the number of degraded segments induced by the λ error of $\pm 10\%$ increases at the beginning of the thermal ageing process and then decreases at a certain ageing time when the number of degraded segments approaches the total number of insulation segments. In an extreme case where all the segments are fully degraded after a sufficiently long thermal ageing process under any degradation rate, the dichotomy models will always give the same IR results independent of degradation rates. For the discretization models which simulate the gradual degradation of individual segments, the IR percentage error amplitudes increase with the ageing time throughout the thermal ageing process and approximately reach 60% for 0.9λ or 40% for 1.1λ at the end of 2000 h. However, the corresponding IR absolute errors at the end of 2000 h are insignificant due to the fact that the IR results become very small after a long thermal ageing time compared with initial IR levels. Since the uncertainty propagating from degradation rates to IR values can be magnified especially when using the discretization models, further exploration should reflect the confidence bounds for IR degradation estimation subject to various sources of uncertainty.

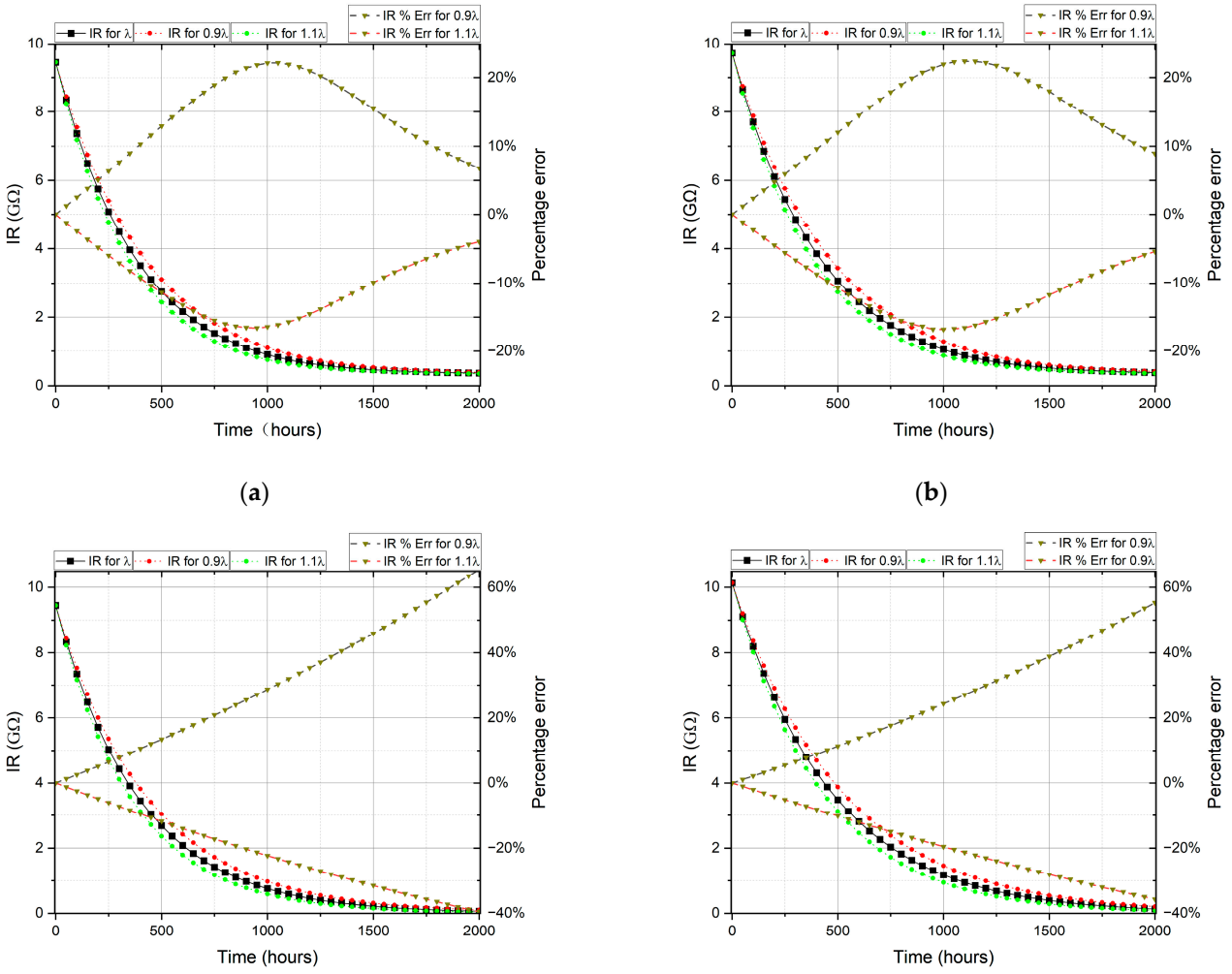

Figure 19. IR degradation trends (Ω) with percentage errors over 2000 h of thermal ageing simulated under uncertain degradation rates by (**a**) dichotomy model with uniform temperature; (**b**) dichotomy model with radial temperature gradients; (**c**) discretization model with uniform temperature; and (**d**) discretization model with non-uniform temperature.

5. Conclusions and Future Work

The insulation of heavily loaded power cables is subjected to varying extents of thermal ageing that causes the degradation of electrical dielectric properties including insulation resistance (IR). To identify an appropriate approach for the IR degradation simulation under thermal ageing, this paper has developed four IR degradation models for cross-linked polyethylene-insulated power cables and compared the IR simulations between different methodologies and also between the uses of uniform and non-uniform temperature profiles. A cylindrical cable insulation sample has been modelled in this work and divided into multiple sufficiently small segments, enabling the random selection of fully degraded segments by dichotomy models and the estimation of individual segment degradation processes by discretization models. The insulation temperature profile has been estimated by modelling the thermal ageing experiment via a finite volume method (FVM) and then refined by an artificial neural network (ANN) to match profile resolutions with the insulation segment sizes.

When assuming a uniform insulation temperature equal to the hotspot temperature of the entire insulation, the dichotomy model has generated lower IR values than the discretization model, especially for a longer thermal ageing duration due to an increased

probability of assigning the fully degraded insulation resistivity to multiple segments that are series connected in the same radial column. Although the incorporation of radial temperature gradients into the dichotomy model has mitigated the overestimation of IR degradation, the resulting IR levels are lower than those that are produced by the discretization model with the exact temperature profile. This is because the discretization model has additionally considered the temperature variation along the longitudinal dimension and simulated the gradual degradation of individual segments separately rather than randomly sampling fully degraded segments from the insulation (layers). In addition, the IR degradation simulation has been performed based on different segment sizes and degradation rates for a sensitivity analysis, suggesting that IR results are more sensitive to the segment size along the radial dimension and to the underestimation of degradation rates. Furthermore, the degree of sensitivity not only varies with the thermal ageing time but also depends on the IR degradation model adopted.

It is noted that the IR degradation models developed here consider thermal ageing effects only. Based on the present work, the proposed discretization model with the full temperature profile should be enhanced to simulate the joint effects of thermal ageing and annealing by additionally considering the diffusion of chemical components from semicon shields which may increase trap density and promote hopping conduction within cable insulation [27]. The cumulation and exhaustion of the chemical components could result in the IR trend exhibiting a U-shape variation at the initial stage of the heating process [28]. Furthermore, the enhanced discretization model will be fitted to laboratory IR measurements to understand the conduction mechanisms in insulation with the presence of semicon layers over the heating process. Moreover, different sources of uncertainty will be translated into the confidence bounds of an IR estimate by simulating their propagation through IR degradation models. In addition, the FVM will be further developed to simulate highly non-uniform insulation temperature profiles which may be induced by local partial discharges and/or complex ambient environments, providing reliable temperature profiles to discretization models for resistivity degradation estimation. The low-resistance current path generated during partial discharges will also be considered in future model development. In the case of overhead cables that are exposed to air, the insulation degradation accelerated by solar radiation should also be explored.

Author Contributions: Conceptualization, B.G.S. and M.J.G.; methodology, X.G. and B.G.S.; software, X.G.; validation, X.G., F.F. and B.G.S.; formal analysis, X.G., F.F. and B.G.S.; investigation, X.G., F.F. and B.G.S.; resources, X.G. and B.G.S.; data curation, X.G. and F.F.; writing—original draft preparation, X.G. and F.F.; writing—review and editing, B.G.S.; visualization, X.G.; supervision, B.G.S. and M.J.G.; project administration, B.G.S.; funding acquisition, B.G.S. All authors have read and agreed to the published version of the manuscript.

Funding: This research was funded by the UK Engineering and Physical Sciences Research Council grant EP-T001445-1.

Data Availability Statement: Data are contained within the article.

Conflicts of Interest: The authors declare no conflicts of interest.

References

1. Klauck, M.; Nobrega, G.; Reinecke, E.A.; Bentaib, A.; Maas, L.; Chaumeix, N.; Allelein, H.J. Experimental investigation on the impact of cable fire products from flame-retardant cables on catalysts used in passive auto-catalytic recombiners. *Prog. Nucl. Energy* **2022**, *152*, 104365. [CrossRef]
2. *IEC Std 60505*; Evaluation and Qualification of Electrical Insulation Systems. IEC Standard: Geneva, Switzerland, 2011.
3. *IEEE Std 1064-1991*; IEEE Guide for Multifactor Stress Functional Testing of Electrical Insulation Systems. IEEE Standard: New York, NY, USA, 1991.
4. Densley, J. Ageing and diagnostics in extruded insulations for power cables. In Proceedings of the 1995 IEEE 5th International Conference on Conduction and Breakdown in Solid Dielectrics, Leicester, UK, 10–13 July 1995; pp. 1–15.
5. Zhou, C.; Yi, H.; Dong, X. Review of recent research towards power cable life cycle management. *IET High Volt.* **2017**, *2*, 179–187. [CrossRef]

6. Boukezzi, L.; Boubakeur, A. Effect of thermal aging on the electrical characteristics of XLPE for HV cables. *Trans. Electr. Electron. Mater.* **2018**, *19*, 344–351. [CrossRef]
7. Mecheri, Y.; Boukezzi, L.; Boubakeur, A.; Lallouani, M. Dielectric and mechanical behavior of cross-linked polyethylene under thermal aging. In Proceedings of the 2000 Annual Report Conference on Electrical Insulation and Dielectric Phenomena, Victoria, BC, Canada, 15–18 October 2000; Volume 2, pp. 560–563.
8. Nedjar, M. Effect of thermal aging on the electrical properties of crosslinked polyethylene. *J. Appl. Polym. Sci.* **2009**, *111*, 1985–1990. [CrossRef]
9. Mecheri, Y.; Bouazabia, S.; Boubakeur, A.; Lallouani, M. Effect of thermal ageing on the properties of XLPE as an insulating material for HV cables. In Proceedings of the International Electrical Insulation Conference, IET Centre, Birmingham, UK, 29–31 May 2013; pp. 29–31.
10. Zhang, C.C.; Li, Y.F.; Hu, M.Y.; Ma, F.L.; Zhao, H.; Han, B.Z. Conductivity properties of XLPE insulation used for HVDC cable after accelerated thermal ageing. In Proceedings of the 2018 12th International Conference on the Properties and Applications of Dielectric Materials (ICPADM), Xi'an, China, 20–24 May 2018; pp. 500–503.
11. Kang, S.D.; Kim, J.H. Investigation on the insulation resistance characteristics of low voltage cable. *Energies* **2020**, *13*, 3611. [CrossRef]
12. Chang, Y.S.; Mosleh, A. Predictive Model on the Degradation of the Electrical Resistance of Cable Insulation. In Proceedings of the Probabilistic Safety Assessment and Management PSAM, Los Angeles, CA, USA, 14 September 2018.
13. DeCarlo, R.A. *Linear Systems: A State Variable Approach with Numerical Implementation*; Prentice-Hall, Inc.: Hoboken, NJ, USA, 1989.
14. Serway, R.A.; Jewett, J.W. Current and resistance. In *Physics for Scientists and Engineers with Modern Physics*, 10th ed.; Cengage: Boston, MA, USA, 2018; pp. 691–712.
15. Rodríguez-Valverde, M.Á.; Tirado-Miranda, M. A simpler derivation of the integral formula of electrical resistance. *Eur. J. Phys.* **2009**, *30*, L47. [CrossRef]
16. Mosleh, A.; Al-Sheikhly, M.; Chang, Y.S.; Reister, R. *Physics-Based Probabilistic Model of the Effects of Ionizing Radiation on Polymeric Insulators of Electric Cables Used in Nuclear Power Plants*; No. 15-8258; University of California: Los Angeles, CA, USA, 2019.
17. Navidi, W.C. *Statistics for Engineers and Scientists*; McGraw-Hill: New York, NY, USA, 2006; p. 2.
18. Stojanović, M.; Klimenta, J.; Panić, M.; Klimenta, D.; Tasić, D.; Milovanović, M.; Perović, B. Thermal aging management of underground power cables in electricity distribution networks: A FEM-based Arrhenius analysis of the hot spot effect. *Electr. Eng.* **2023**, *105*, 647–662. [CrossRef]
19. *IEEE 1407-2007*; IEEE Guide for Accelerated Aging Tests for Medium-Voltage (5kV–35kV) Extruded Electric Power Cables Using Water-Filled Tanks. Power Engineering Society: New York, NY, USA, 2007; Sponsored by the Insulated Conductors Committee.
20. Meng, X.K.; Wang, Z.Q.; Li, G.F. Dynamic analysis of core temperature of low-voltage power cable based on thermal conductivity. *Can. J. Electr. Comput. Eng.* **2016**, *39*, 59–65. [CrossRef]
21. Lee, K.Y.; Yang, J.S.; Choi, Y.S.; Park, D.H. Specific heat and thermal conductivity measurement of XLPE insulator and semi-conducting materials. In Proceedings of the 2006 IEEE 8th International Conference on Properties & Applications of Dielectric Materials, Bali, Indonesia, 26–30 June 2006; pp. 805–809.
22. Jia, Y.; Mao, Z.; Huang, W.; Zhang, J. Effect of temperature and crystallinity on the thermal conductivity of semi-crystalline polymers: A case study of polyethylene. *Mater. Chem. Phys.* **2022**, *287*, 126325. [CrossRef]
23. Gray, D.D.; Giorgini, A. The validity of the Boussinesq approximation for liquids and gases. *Int. J. Heat Mass Transf.* **1976**, *19*, 545–551. [CrossRef]
24. The Engineering Toolbox. Air—Density, Specific Weight and Thermal Expansion Coefficient vs. Temperature and Pressure. Available online: https://www.engineeringtoolbox.com/air-density-specific-weight-d_600.html (accessed on 16 November 2021).
25. Ge, X.; Given, M.J.; Stewart, B.G. Determining accelerated aging power cable spatial temperature profiles using Artificial Neural Networks. In Proceedings of the 2022 IEEE International Conference on High Voltage Engineering and Applications (ICHVE), Chongqing, China, 25–29 September 2022; pp. 1–4.
26. Beale, M.H.; Hagan, M.T.; Demuth, H.B. *Deep Learning Toolbox*; User's Guide; The MathWorks, Inc.: Natick, MA, USA, 2018.
27. Diego, J.A.; Belana, J.; Orrit, J.; Cañadas, J.C.; Mudarra, M.; Frutos, F.; Acedo, M. Annealing effect on the conductivity of XLPE insulation in power cable. *IEEE Trans. Dielectr. Electr. Insul.* **2011**, *18*, 1554–1561. [CrossRef]
28. Ge, X.; Fan, F.; Given, M.J.; Stewart, B.G. XLPE cable insulation resistance modelling under annealing and thermal ageing effects. In Proceedings of the 98th IEEE Conference on Electrical Insulation and Dielectric Phenomena, East Rutherford, NJ, USA, 15–19 October 2023.